1   **Determining finite strain: how far have we progressed?**

2   Dave McCarthy[1], Patrick Meere[2] and Kieran Mulchrone[3]

3   1 British Geological Survey, The Lyell Centre, Research Avenue South, Edinburgh, EH14 4AP, UK

4   2 School of Biological, Earth and Environmental Sciences, University College, Cork, Ireland

5   3 Department of Applied Mathematics, University College, Cork, Ireland

6   **Abstract**

7   One of the main aims in the field of structural geology is the identification and quantification of

8   deformation or strain. This pursuit has occupied geologists since the 1800's, but has evolved

9   dramatically since those early studies. The quantification of strain in sedimentary lithologies was

10   initially restricted to lithologies of known initial shape, such as fossils or reduction spots. In 1967,

11   Ramsay presented a series of methods and calculations, which allowed populations of clasts to be

12   used as strain markers. These methods acted as a foundation for modern strain analysis, and have

13   influenced thousands of studies. This review highlights the significance of Ramsay's contribution to

14   modern strain analysis. We outline the advances in the field over the 50 years since publication of the

15   'Folding and Fracturing of Rocks', review the existing limitations of strain analysis methods and look

16   to future developments.

17

18   *'The analysis of the variation in amount of finite strain in a deformed zone is of the utmost importance*

19   *in helping to understand the structural geometry and hence the structural history of the rocks.'*

20   *John Ramsay, 1967*

21   The field of structural geology is primarily concerned with understanding the deformation of crustal

22   rocks. This deformation or strain is caused when external forces or stresses act on a rock mass, causing

23   a change in its shape or size (Ramsay, 1967). The concept of quantifying strain in rocks has been

24   prevalent since the 1800's, and has evolved dramatically since those early studies. Various methods

25   have been used to identify and quantify strain, the earliest of which relied on objects of a known initial

26 shape. This approach was first taken by Phillips (1843) and Sharpe (1847) who used deformed fossils,

27 with Sharpe (1847) noting that the most deformed fossils were present in the areas with the most

28 intense cleavage. This led to Sorby's seminal interpretations of cleavage development (Sorby, 1849)

29 and correlation of cleavage to areas with high strain (Sorby, 1856). Haughton (1856) provided the first

30 mathematical description of length changes in fossils due to strain in naturally deformed rocks,

31 furthermore, he applied the concept of the strain ellipsoid to rock deformation, which established a

32 framework for strain to be quantified and compared.

33 It was not until the quantitative studies on distorted ooids by Cloos (1947) that truly numerical and

34 methodological strategies were fully applied to strain analysis. By the early 1960's, strain analysis

35 methods were still largely dependent on the presence of strain markers of known initial shape, such

36 as fossils, ooids or reduction spots (Breddin, 1954, 1957; DeSitter, 1964). In 1967, John Ramsay

37 presented a suite of precise and mathematical procedures that allowed for the accurate

38 determination of finite strain in deformed rocks. These methods, though significantly modified, have

39 stood the test of time and are regularly employed. Of the many publications citing Ramsay's Folding

40 and Fracturing, a significant number, >1000, have focussed on strain analysis (Lisle, this issue). It is

41 clear that these techniques are still applied to both field studies and mathematical models of rock

42 deformation.

43 This review starts by highlighting the importance of Ramsay's initial contribution, then we outline the

44 significant advances in the techniques of strain analysis made over the last 50 years. This is followed

45 with a brief discussion on applications of strain analysis and how these techniques have advanced our

46 understanding of natural rock deformation. There is clearly a huge body of research involving strain

47 analysis and it is not possible to reference every application here, but we have highlighted some key

48 developments. We then follow this by providing a discussion of some of the key unresolved problems

49 in the field. We conclude with some ideas for future directions and hope that this will act as a

50 springboard for those investigating strain in rocks for the first time.

51 **Strain Analysis Techniques proposed by Ramsay**

52 The significance of Ramsay's contribution was that he set out in a systematic and mathematical

53 manner techniques for determining strain from objects of known initial shape, and he established

54 methods which allowed populations of objects, such as sedimentary clasts, of non-spherical and

55 fluctuating initial shape, to be used as strain markers. These methods depend on clast orientation,

56 repacking and intraclast deformation of clasts due to deformation. This was a key development in

57 strain analysis, as it allowed estimates to be made from lithologies that did not have obvious or

58 established strain markers (Fig. 1). The methods developed by Ramsay (1967) are briefly outlined

59 below:

60 *Method 1*

61 The first method that Ramsay outlined built on existing techniques at the time, and involved direct

62 measurement of the principal axes of elliptical strain markers and the orientation of their long axes

63 (Ramsay, 1967, p 193). These axes are then plotted against each other (Fig. 2a) and the slope of the

64 best-fit line that also passes through the origin provides an estimate of the strain ratio (Fig. 2b).

65 Ramsay noted it was difficult to accurately identify ellipse lengths in high deformation regimes, and

66 that it was difficult to identify the maximum stretching direction in low strain regimes.

67 *Method 2*

68 The second method (Ramsay, 1967, p 193-194), does not rely on direct measurement of ellipse axes,

69 and accounts for difficulties in methods of identifying the length of maximum ellipse axes. The centre

70 of each ellipse is identified and the lengths of chords from the centre to the edge of each ellipse along

71 three arbitrarily directions are measured. The sum of the chord lengths for the three defined

72 directions for a population of objects is calculated (Fig. 2c). If the objects were initially circular, the

73 ratios of elongation can be calculated for each direction.

74

75   *Method 3*

76   This method, commonly referred to as the nearest-neighbour or centre-to-centre method, (Ramsay,

77   1967, p 195-196) was developed to tackle cases where pressure solution was suspected to have

78   occurred, and is applicable to rocks with particles equally or unequally distributed throughout the rock

79   mass. In cases where pressure solution is a significant deformation mechanism, the elliptical shape or

80   preferred orientation of markers is not reliable. This method is particularly useful for identifying cases

81   where non-passive deformation is thought to have occurred (i.e. that the clasts are not deforming

82   homogeneously with the matrix). The basic premise involves measuring the distance between object

83   centres, and assuming that in the unstrained state these distances should be isotropic (Fig. 3a). During

84   deformation the distance between centres should become shorter parallel to the maximum

85   compression axis (Fig. 3b & c).

86   *Method 4*

87   The fourth method (Ramsay, 1967, p 197-199) utilised the measurements of distorted angles of radial

88   and tangential lines in elliptical sections, such as those in spherulites. Whilst an elegant method of

89   calculating strain, this method has had limited use due to the specific nature of the strain markers

90   required.

91      $R_f/\emptyset$ *Method*

92   In addition to the four methods above, Ramsay (1967, p 204-211) also outlined a method for

93   specifically dealing with markers of initial elliptical, the $R_f/\emptyset$ method (Fig. 4), where R_f is the deformed

94   axial ratio of the marker ellipsoid, while $\emptyset$ is the orientation of the long axis. This is slightly more

95   complex than using initially circular objects, in that when an ellipse is deformed under homogeneous

96   conditions, the resulting shape is another ellipse. The axial ratio (R_f) and orientation of the deformed

97   ellipse is a result of the combination of the initial aspect ratio (R_i) and orientation (θ), and the strain

98   ellipse, all of which are unknowns. When a population of deformed ellipses are considered, variations

99   in their Ø values can be related to eccentricity in their orientations prior to deformation.

100   **Measuring strain after Ramsay**

101   Essentially Ramsay (1967) developed methods whereby strain estimates could be made using

102   parameters derived from the following: strain marker orientation, strain marker shape, position of

103   strain marker centres, distance between centres and the angle between centres. The two main types

104   of methods that prevailed were the $R_f/\emptyset$ method and the centre-to-centre. The $R_f/\emptyset$ method (Fig. 4)

105   determines finite strain from randomly oriented populations of deformed elliptical objects, while the

106   centre-to-centre method (Fig. 3) uses the distance between centres of adjacent objects, and assumes

107   the objects were uniformly distributed prior to deformation.

108   Subsequent to the initial $R_f/\emptyset$ method, alternative methods based on marker shape and orientation

109   were developed (Dunnet, 1969; Elliott, 1970; Dunnet and Siddans, 1971; Matthews et al., 1974;

110   Borradaile, 1976; Shimamoto and Ikeda, 1976; Lisle, 1977a, 1977b, 1985; Robin, 1977; Peach and Lisle,

111   1979; Siddans, 1980; Yu and Zheng, 1984; Mulchrone and Meere, 2001; Mulchrone et al., 2003).

112   Dunnet (1969) developed an $R_f/\emptyset$ diagram method, while Elliott (1970) applied a similar graphical

113   approach, the shape factor grid. Dunnet and Siddans (1971) took non-random initial orientations into

114   consideration for the $R_f/\emptyset$ diagram method. A significant drawback of these methods is that they are

115   subjective.

116   An algebraic method that accommodated statistical analysis of any errors produced was introduced

117   by Matthews et al. (1974). The drawback of this method was that the orientation of the principal strain

118   axis needed to be calculated independently prior to using the method. Similarly, Robin (1977) derived

119   a method that allowed analysis of strain markers of any shape but required prior independent

120   knowledge of the principal strain axes. Advances in the $R_f/\emptyset$ method are discussed in further detail by

121   Lisle (1994). In order to address the issues outlined above with calculating strain from distributions of

122   elliptical objects, Shimamoto and Ikeda (1976) developed an objective non-graphical, reproducible

123 approach to strain analysis. This approach averaged the parameters of all of the marker ellipses to

124 generate one marker ellipse, or if the initial distribution was isotropic, a marker circle. The Mean Radial

125 Length (MRL) method of Mulchrone et al. (2003) took a similar approach, whereby the average shape

126 of a population of isotropic ellipses or non-deformed sedimentary clasts equates to a circle. As this

127 population becomes deformed by either shape change or rotation, this circle becomes an ellipse

128 and can be directly related to the strain ellipse in the same manner that any circular marker can

129 after deformation.

130 The centre-to-centre family of techniques are based on using object-to-object separation and assume

131 that the distribution of marker objects are isotropic and that after deformation the distance between

132 any marker centre and all other clast centres has been modified. The relative change in clast centres

133 distances can be related to the direction and magnitude of the finite strain ellipse (Ramsay, 1967).

134 Compared to the Rf/Ø method, the centre-to-centre method involved relatively complicated

135 calculations and was particularly labour intensive. As a result, it initially received significantly less

136 attention than the Rf/Ø method. This changed when a relatively simple graphical approach was

137 developed by Fry (1979; Hanna and Fry, 1979), which used all object-object separations. This was

138 subsequently further improved as the Normalised Fry Method (Erslev, 1988) and the enhanced

139 Normalised Fry Method (Erslev and Ge, 1990). McNaught (1994) further extended these methods by

140 facilitating the use of non-elliptical markers by determining best-fit ellipses for these irregular shaped

141 objects. One of the drawbacks of the centre-to-centre techniques is that they do not account for

142 volume loss, which can be considerable when pressure solution is a dominant deformation mechanism

143 (Onasch, 1986; Dunne et al., 1990). Furthermore, if pressure solution is significant, there are

144 difficulties in identifying the pre-strain centres of clasts and if significant heterogeneous deformation

145 is present at the clast scale than this can lead to further underestimates of strain.

146 The Fry methods have been regularly incorporated into automated analysis tools (Ailleres et al., 1995;

147 Launeau and Robin, 1996; Launeau et al., 2010). Despite popularity and ease of use, these methods

148 are subjective, with interpreter bias being introduced at both the identification of clast centres, and

149 the definition of the central ellipse on the Fry plot. Mulchrone (2003) used Delaunay triangulation to

150 characterise nearest neighbour separations, and defined object centres using the centroid of the best-

151 fit ellipse. This resulted in a more objective and automated process for identifying object centres and

152 creating the tie-lines between nearest neighbours.

153   *Calculating the strain ellipsoid*

154 Most strain analysis techniques focus on quantifying strain in a 2D plane. In order to quantify strain in

155 3D, a strain ellipsoid needs to be defined. Typically, the strain ellipsoid is defined from strain ellipses

156 on several planar surfaces with differing orientations. Similar to calculating the strain ellipse,

157 calculating the strain ellipsoid is not a trivial process, and numerous attempts have been made at

158 determining the most accurate best-fit ellipsoid. Ramsay (1967; p. 142-147) derived a series of

159 equations to solve for the best-fit ellipsoid from three mutually perpendicular planes. Numerical

160 algorithms were subsequently developed for three orthogonal sections (Shimamoto and Ikeda, 1976;

161 Oertel, 1978). This was followed by methods, which allowed for non-orthogonal sections (Milton,

162 1980; Gendzwill and Stauffer, 1981; Shao and Wang, 1984; De Paor; 1990). Owens (1984) in particular

163 described an iterative method for the calculation of the best-fit strain ellipsoid from any number of

164 non-perpendicular sections using a least squares approach, as well as applying a scale factor. Robin

165 introduced an approach utilising a series of linear equations (Robin, 2002; Launeau and Robin, 2005).

166 Shan (2008) built on the Robin method, and included added flexibility, whereby stretching lineation

167 data could be included. The important distinction of the Robin and Shan methods from the previous

168 methods was that they were non-iterative but separated the parameters to be calculated from the

169 initial data. Vollmer (2017) has provided a more detailed comparison of the Robin and Shan methods,

170 as well as applying bootstrap statistics to the results. Mookerjee and Nickleach (2011) presented a

171 suite of methods in Mathematica, which attempts to minimise the errors between the best-fit ellipsoid

172 and any of the measured planes used as input data.

173 *Graphical representation of the strain ellipsoid*

174 The geometries of strain ellipsoids can be represented in 2D space using a Flinn Plot (Flinn, 1956, 1962,

175 1965). This type of plot was first used to compare the elliptical properties of clast populations in

176 conglomerates (Zingg, 1935). The ratio of the maximum to intermediate ellipsoid axes (R X/Y) is

177 plotted as ordinate and the ratio of the minimum to intermediate axes (R Y/Z) is plotted as abscissa

178 on these graphs. The Flinn Plot was subsequently modified by Ramsay (1967) to include a logarithmic

179 scale (Fig. 5; discussed further in Hobbs et al., 1976; Ramsay and Huber, 1983). The benefit of the

180 logarithmic Flinn Plot is that it provides a more even distribution of points with increase in deformation

181 (Ramsay and Huber, 1983), whilst in the original Flinn Plot low strains are clustered near the origin,

182 making it difficult to interpret data.

183 The symmetry of the strain ellipsoid can be described by the ratio K ((X/Y)/(Y/Z)). If K>1 then the

184 ellipsoid is considered to have a prolate or axial symmetric constriction and has one long axis and two

185 shorter axes. If K<1 the ellipsoid is considered to be oblate or axially symmetrically flattened and has

186 two long axes and one shorter axis. Between these two fields of flattening and constriction is the field

187 of plane strain (K=1) and which only occurs when strain is acting in the XZ plane. K represents the slope

188 of a line from the data point to the origin at (1,1), so that K=a-1/b-1 with a=x/y and b=y/z. K on the

189 diagram can define a series of domains, so that when K=0 the finite strain ellipsoid is uniaxial oblate

190 and has been flattened perpendicular to Z. As K tends towards 1 the ellipsoid moves away from being

191 purely uniaxial, but remains in the oblate and flattened domain. For K values greater than 1 the

192 ellipsoid lies in the prolate or constrictive domain, and for K=∞ the ellipsoid is purely uniaxial prolate

193 and stretched along the X axis (Park, 1997). The degree of how far removed the ellipsoid is from

194 spherical (ellipsoid eccentricity) is calculated as $\sqrt{((X/Y)2 + (Y/Z)2)}$.

195 A less-popular alternative to the Flinn Plot, the Nadai-Hsu Plot (Fig. 5; Nadai, 1950; Hsu, 1966) was

196 first applied to geological strain analysis by Hossack (1968). This type of plot presents strain in a polar

197 area, and is argued to provide a less distorted representation of the deviatoric strains (Hobbs et al.,

198   1976; Brandon, 1995; Mookerjee and Peek, 2014). Another advantage of this type of polar plot is that

199   ellipsoids with low strain ratios plot closer together regardless of the ellipsoid shape. Ramsay and

200   Huber (1983) criticised the Nadai-Hsu plots, irrotational strain is assumed, while most natural

201   deformation involves progressive non-coaxial rotational strains.

202   The fundamental difference is that the Nadai-Hsu Plots use the *amount of strain* (εs) and Lode's Ratio

203   (v), to define the ellipsoid shape (Lode, 1926). The *amount of strain*, is related to the octahedral shear,

204   Υo, and is defined by: $\varepsilon s = (\sqrt{3} / 2) \Upsilon o$, where $\Upsilon o = (2/3) [(\varepsilon 1 - \varepsilon 2)^2 + (\varepsilon 2 - \varepsilon 3)^2 + (\varepsilon 3 - \varepsilon 1)^2]^{\frac{1}{2}}$ and $\varepsilon 1$,

205    $\varepsilon 2$ and $\varepsilon 3$ represent the strain axes. The Lode Ratio is defined as $v = (2\varepsilon 2 - \varepsilon 1 - \varepsilon 3) / (\varepsilon 1 - \varepsilon 3)$ and

206   ranges from -1 to 1. Lode ratios of -1 define a prolate ellipsoid, while 1 and 0, define an oblate and

207   plane strain ellipsoid respectively. Whereas the Flinn Plot solely relies on the aspect ratios of the strain

208   ellipsoid (as discussed above). For a more in depth discussion of the merits of each method readers

209   are referred to Mookerjee and Peek (2014) and Vollmer (2017).

210   *Automation*

211   Possibly one of the biggest drawbacks to most strain analysis studies is the high labour intensity

212   required for both the identification of object boundaries, and the accurate identification of their

213   centres for enough objects to create a statistically robust sample set. Since the late seventies, many

214   attempts have been made at automating strain or fabric analysis to address this (e.g., Peach and Lisle,

215   1979). Initially, the limiting steps in the automation of these strain analysis techniques was the

216   recognition and fitting of best-fit ellipses to geological strain markers, such as sedimentary clasts (Fig.

217   6a & b).

218   The efficient and accurate automatic segmentation of thin section images is still a developing field and

219   has received a lot of recent attention with numerous attempts at automated extraction using image

220   processing or GIS-based techniques (e.g., Goodchild and Fueten, 1998; Heilbronner, 2000; van den

221   Berg et al., 2002; Perring et al., 2004; Barraud, 2006; Choudhury et al., 2006; Li et al., 2008; Tarquini

222   and Favalli, 2010; DeVasto et al., 2012; Gorsevski et al., 2012; Heilbronner and Barrett 2013;

223   Mingireanov Filho et al., 2013; Jungmann et al., 2014; Asmussen et al., 2015). Although these methods

224   produce rapid grain boundary maps, they are typically inaccurate or achieve different results

225   depending on the nature of the image. This is highlighted by the regular use of quartz clasts as strain

226   markers, whereby the automatic identification of their boundaries is complicated by undulose

227   extinction, deformation bands, diffuse boundaries and colour similarities between neighbouring

228   grains. Despite these advances, most methods follow the approach of Mukul (1998), whereby grains

229   used as strain markers are manually traced, and then analysed using image analysis software.

230   A number of methods for automated image analysis have been successfully utilised in the past for

231   geological strain analysis (Ailleres et al., 1995; Erslev and Ge, 1990; Masuda et al., 1991; McNaught,

232   1994; Heilbronner and Barrett, 2013). Panozzo (1984) utilised digitised sets of points representing

233   linear or elliptical objects in her projection method. Mulchrone et al. (2005) developed a parameter

234   extraction program (SAPE) that rapidly extracts the required data by using a simple region-growing

235   algorithm to identify regions of interest. Vollmer developed a similar method, Ellipsefit (Vollmer, 2010,

236   2011, 2017). Many of these techniques are discussed in Heilbronner and Barrett (2013), who have

237   provided a superb overview of image analysis techniques for geological material and it is

238   recommended as a starting point for readers interested in this field.

239   Once grain boundaries have been identified and ellipses are fitted to clasts, the parameters required

240   for a range of strain analysis techniques such as the aspect ratio, orientation, and the centroid of the

241   object can now be easily extracted. For the Rf/Ø method the difficulties in calculating a strain estimate

242   cease once ellipses have been fitted to strain markers; for the centre-to-centre methods the

243   difficulties continue.

244   The accuracy of centre-to-centre strain estimates can be further hampered by the ability to clearly

245   define the vacancy field or central void of the Fry Plot (Fig. 6c), which in a strained sample should

246   represent the strain ellipse (Crespi, 1986; Waldron and Wallace, 2007). A variety of techniques have

247   been applied in order to accurately and objectively define this void (Erslev and Ge, 1990; McNaught,

248   1994; Waldron and Wallace, 2007; Lisle, 2010; Shan and Xiao, 2011; Reddy and Srivastava, 2012;

249   Mulchrone, 2013). Similar problems exist for defining the curve of the polar plot (Mulchrone, 2013).

250   In order to reduce the time and labour intensity required, Mulchrone et al. (2013) integrated image

251   analysis, ellipse fitting and parameter extraction, and strain analysis routines for MRL and DTNNM in

252   one workflow. They also included a method for bootstrapping the results in order to produce

253   uncertainty estimates (Fig. 6 e&f). Kumar et al. (2014) carried out a detailed comparison analyses on

254   these methods, and found that the Delaunay Triangulation Method of Mulchrone (2013) and the

255   Continuous Function Method of Waldron and Wallace (2007) were the most accurate. Additionally

256   they concluded that the Delaunay Triangulation Method and the image analysis technique of Reddy

257   and Srivastava (2012) were the most time efficient.

258   The other method that has stood out is the SURFOR method, first presented by Panozzo (1984, 1987),

259   and discussed in detail in Heilbronner and Barrett (2013). The SURFOR method takes a slightly

260   different approach to fabric or strain analysis compared to the Ramsay family of methods. Rather than

261   focussing on the object orientation or the spatial relationship between objects, the SURFOR method

262   quantifies the fabric based on the shape, size and orientation of 'surfaces' (Heilbronner and Barrett,

263   2013). The 'surfaces' can be any linear element, such as fractures or grain boundaries. One particular

264   advantage of the SURFOR method over the original Ramsay Rf/Ø method is that it accounts for marker

265   size, with smaller objects having less of an impact on the final strain/anisotropy estimate. A similar

266   approach is taken by Launeau et al. (1990, 1996, 2010), whereby linear filters are used to count

267   intercepts along any arbitrary direction of a digital image. The intercepts technique has shown to be

268   comparable to the MRL and the DTNNM methods in moderate strain regimes, although in low strain

269   regimes there appears to be a discrepancy between the methods (McCarthy et al., 2015). These

270   discrepancies are due to uncertainties in strain estimates in low strain regimes.

271

272 **Application of strain analysis and advances in strain theory**

273 This contribution has focussed on the significant advances made in geological strain analysis, as

274 outlined above, which have provided a number of valuable insights into geological deformation.

275 Unfortunately, natural deformation is rarely simple or restricted to 2D planes, yet this approach have

276 aided with understanding of complex deformations.

277 Strain analysis and resulting knowledge of the finite strain state of a point in a rock mass has played a

278 fundamental part in the understanding of the development of tectonic fabrics and foliations (Ramsay

279 and Wood, 1973, Tullis and Wood, 1975). However, nature tends to reveal more by capturing change

280 in strain through time and space, (e.g. porphyroclasts and related structures, layers which are

281 shortened and then stretched, and regions of intense shear where the continuum from low to high

282 strain can be spatially traced). Often the spatial changes can be interpreted as reflecting the temporal

283 deformation history. Ramsay (1967) applied the concept of infinitesimal strain together with that of

284 finite strain to understand deformation history, with the difference between what happens in a short

285 time step compared to that over long time periods helped develop the ideas of progressive strain. This

286 infinitesimal approach was followed by the seminal work of Means et al. (1980) who considered the

287 velocity gradient tensor to conceptualise progressive deformation, and used vorticity to quantify

288 rotational deformation. A detailed discussion of vorticity is beyond the scope of this contribution, and

289 interested readers should consult the work of Fossen and Tikoff (Fossen and Tikoff, 1993; Tikoff and

290 Fossen, 1993; Tikoff and Fossen, 1995; Tikoff and Fossen, 1999; Passchier and Trouw, 2005).

291 Many of the 2D finite strain methods discussed in previous sections have a natural extension to 3D,

292 but there is still a dearth of 3D strain studies. Methods based on shape (e.g. Shimamoto and Ikeda,

293 1976; Mulchrone et al., 2003) and inter-object relationships (e.g. Fry, 1979; Mulchrone, 2013) can be

294 readily developed into 3D methods. However, in many cases the primary difficulty rests with acquiring

295 suitable data in 3D in order to apply the methods. Recent technological advances have seen the

296 application of tomography to the acquisition of high quality images of 3D markers in rocks (Louis et al,

297   2006; Adam et al, 2013; Robin and Charles, 2015). This is certain to be an area of future development

298   and will inform finite strain studies and their interpretation in the context of 3D deformation history

299   (Tikoff and Fossen, 1999).

300   Important comparisons have been made between clast-based strain analyses and other methods of

301   quantifying deformation. A number of studies in the seventies and eighties highlighted a close

302   relationship between finite strain estimates and quartz crystallographic fabrics (Marjoribanks, 1976;

303   Miller and Christie, 1981; Lisle, 1985; Law, 1986). Rapid developments in techniques such as Electron

304   Back Scatter Diffraction (EBSD) have largely confirmed this relationship, but also provided insights into

305   deformation at subgrain scales one of the most prominent methods for the determination of preferred

306   orientation of minerals in thin sections (Passchier and Trouw, 2005; Prior et al., 2009).

307   Similar advances in rock deformation studies have been made in the field of Anisotropy of Magnetic

308   Susceptibility (AMS), with Graham (1954) first suggesting that magnetic fabrics could be a valuable

309   tool in petrofabric analysis and establishing a link between layer parallel shortening and AMS. Since

310   this pioneering study there has been a huge volume of work confirming the ability of AMS to

311   determine the orientation-distribution of all minerals and all subfabrics in a specimen, with

312   comprehensive reviews provided by Borradaile and Henry (1997) and Borradaile and Jackson (2010).

313   In direct comparisons of AMS to strain analysis techniques, AMS has been shown to be a highly

314   sensitive and rapid method for quantifying tectonic fabrics (Burmeister et al., 2009; Weil and Yonkee,

315   2009; McCarthy et al., 2015).

316   Other significant contributions of strain analysis includes providing accurate information for structural

317   restorations. Compaction and stratigraphic thickening due to deformation can be estimated and

318   incorporated in the construction of balanced cross sections (Woodward et al., 1986; Protzman and

319   Mitra, 1990; Mitra, 1994). Despite Layer Parallel Shortening (LPS) or internal deformation

320   (compaction, collapse of pore space, dissolution or cleavage formation) being shown to accommodate

321   significant shortening in balanced cross sections from carbonate duplexes (27%; Cooper et al., 1983),

322   gravity driven thrust systems (18-25%; Butler and Paton, 2010), and analogue models (15-30%; Koyi

323   et al., 2004; Burberry, 2015; Lathrop and Burberry, 2017), strain analysis techniques are rarely applied

324   to balancing cross sections.

325   **Unresolved issues in strain analysis**

326   Hobbs and Talbot (1966) highlighted a few of the limitations of strain analysis a year before Ramsay

327   published his seminal text, and the majority of these seem to prevail today: the initial shapes of many

328   strain markers cannot be measured accurately enough to yield highly accurate estimates; and

329   homogeneous strain is typically assumed. Although these assumptions still prevail, they have largely

330   been accepted to be unresolved. In addition to this, a number of factors add further uncertainty to

331   any strain estimate including: strength and influence of the primary or pre-strain fabric; effects of non-

332   passive strain; and the effects of volume-change, these are discussed below.

333   *Primary fabrics*

334   The largest problem for strain analysis methods is the uncertainty regarding the strength and

335   orientation of an initial primary fabric. Most strain analysis methods, particularly the $R_f/\emptyset$ family of

336   techniques, rely on the assumption that the strain markers have a random initial orientation. Certainly

337   in the case of sedimentary rocks this is rarely true, as most sediments develop a preferred orientation

338   either due to depositional processes or diagenesis (Elliott, 1970; Dunnet and Siddans, 1971; Boulter,

339   1976; Seymour and Boulter, 1979; De Paor, 1980; Holst, 1982; Paterson and Yu, 1994; Maffione and

340   Morris, 2017).

341   In a study of undeformed lithologies Holst (1982) found that sections not parallel with bedding had a

342   preferred orientation of clasts along the trace of the bedding plane, while sections parallel to bedding

343   typically had no preferred orientation of clasts. Even if an isotropic or random depositional fabric

344   existed, a preferred orientation typically develops during diagenesis and compaction through active

345   or partly rigid body rotation (Borradaile, 1987). Several efforts have been made to remove the effects

346   of primary fabrics on strain estimates (Elliott, 1970; Dunnet and Siddans, 1971; Matthews et al., 1974;

347   Shimamoto and Ikeda, 1976; Lisle, 1977a; Seymour and Boulter, 1979; Holst, 1982; Wheeler, 1986;

348   DePaor, 1988). Unfortunately, most of these methods utilise one or more of the above assumptions

349   and/or assume the existence of independent information concerning the strain ellipsoid. Some of

350   these assumptions regarding the primary fabrics of sedimentary rocks were highlighted by Patterson

351   and Yu (1994) and include the following: individual grains are spherical prior to straining; orientations

352   and shapes of grain populations define spherical, pre-strain fabric ellipsoids (i.e. grains have an initial

353   uniform distribution); pre-strain fabric ellipsoids are symmetric around bedding; and initial fabrics are

354   recognisable even after straining.

355   Failing to account for any of these factors can lead to considerable errors in strain estimates,

356   particularly in domains with relatively low strains (R <1.5). To account for these errors Patterson and

357   Yu (1994) suggested that a correction should be applied by multiplying the estimated strain ellipsoid

358   by an average pre-strain ellipsoid. Unfortunately, information regarding the magnitude and

359   orientation of the pre-strain ellipsoid is rarely available. Paterson and Yu (1994) compiled XYZ averages

360   for a range of rock types, but this is a limited data set and should be expanded. Regarding the

361   orientation, the estimated strain ellipsoid can be multiplied by the reciprocal pre-strain ellipsoid

362   multiple times in numerous orientations to create an error bracket. Ramsay (1967) showed that all

363   possible combinations of two ellipsoids result in an approximate triangular region on a Flinn plot.

364   Following the methodology of Paterson and Yu (1994), this triangular region is then representative of

365   the error bars of the strain estimate.

366

367   *Non-passive deformation*

368   A key assumption of most current strain analysis techniques is that strain is homogenous and that

369   markers behave in a wholly passive manner in relation to their host material. This breaks down in most

370   natural materials especially when sedimentary clasts are used for strain analysis.

371   Clearly, the most ideal strain markers are those that were originally spherical, which were then

372   deformed passively with no competency contrast between the marker and the host rock. If this holds

373   true then the final shape of the marker will reflect that of the finite strain ellipsoid (Ramsay, 1967).

374   The fundamental assumption of most strain analysis methods is that there is no competency or

375   ductility contrast between the markers and their matrix/host rock, so that the marker and surrounding

376   rock matrix responded to deformation identically. Unfortunately, clasts and their surrounding matrix

377   rarely deform in a passive manner, due to competency or ductility contrasts between the marker and

378   the host rock. This competency contrast is inherently linked to the viscosity contrast between different

379   clast types and the matrix (Ramsay, 1967; Gay, 1968a,b, 1969; Lisle, 1985b; Freeman, 1987; Freeman

380   and Lisle, 1987; Treagus, 2002; Mulchrone and Walsh, 2006; Czeck et al., 2009). Gay (1968a) pointed

381   out that clasts with a low viscosity deform faster than the bulk rock strain ellipse, while clasts with

382   high viscosities resisted deformation and deformed slower than the bulk rock strain ellipse. Gay

383   (1968a) also noted that the viscosity ratio between a clast and the matrix is dependent on the relative

384   proportion of clasts and matrix. Freeman and Lisle (1987) confirmed that the errors in strain estimates

385   are higher when the clasts represent a small fraction of the bulk rock. This is driven by the high ductility

386   contrast, whereby the majority of strain is accommodated by the weaker matrix. As the clast-to-matrix

387   ratio increases the ductility contrast reduces, potentially caused by the reduced ability of the matrix

388   to flow due to the increase in clast on clast interaction. This separation of strain behaviour between

389   the matrix and clasts is typically termed strain partitioning. This type of behaviour is largely controlled

390   by object concentration and the degree of packing and clast interaction, due to the effect these have

391   on the viscosity contrasts (Gay, 1968a; Lisle et al., 1983; Mandal et al., 2003; Vitale and Mazzoli, 2005).

392   Generally, lithologies with higher object concentrations display reduced effects of strain partitioning,

393   leading to more accurate strain estimates (Mandal et al., 2003; Vitale and Mazzoli, 2005).

394   While reviewing problems arising from these competency contrasts, Treagus and Treagus (2002)

395   concluded that conglomerates as a whole deformed at an approximately constant viscosity in a

396   linearly viscous manner, but also found that Rf/Ø style methods characterised clast strain whereas the

397   centre-to-centre methods were more effective at characterising bulk rock strain. This is in part due to

398   two factors: clasts typically only represent 50-70% of the bulk rock (Leeder, 1982); and the Rf/Ø

399   methods only consider clast shape and orientation, while centre-to-centre techniques account for

400   distances between the clasts.

401   This non-passive deformation can be accounted for by utilising centre-to-centre methods, which

402   include spatial information in the estimates of strain, and provide bulk-rock strain estimates that are

403   closer to true strain values. This has been illustrated in a range of natural settings (Meere et al., 2008,

404   Soares and Dias, 2015). Meere et al. (2008) attributed non-passive deformation to the presence of a

405   relatively incompetent clay-rich matrix, which effectively cushioned clasts from internal deformation.

406   This type of behaviour allows for high degrees of competent clast long-axis alignment achieved by a

407   combination of rigid body rotation, layer boundary slip and particle–particle interactions, with

408   minimal evidence of penetrative deformation, despite evidence from traditional strain markers such

409   as reduction spots and deformed burrows (Meere et al., 2008). In these situations, using the Rf/Ø

410   methods leads to a significant underestimate of strain. More recently, Meere et al. (2016) highlighted

411   the importance of identifying passive clast behaviour and the potential for deformation prior to

412   lithification in understanding the deformation history of a region.

413

414 *Volume change*

415 Most studies applying the strain analysis techniques discussed, do not account for any potential

416 volume change of the markers. Although Ramsay (1967) had already presented a modified Flinn

417 diagram, which was capable of including some aspect of volume loss, this aspect of strain analysis is

418 typically ignored. Clearly natural deformation rarely occurs in a closed system, and many attempts

419 have been made at estimating volume reduction during deformation, as opposed to diagenetic

420 volume loss. For example, there has been considerable debate regarding the amount of volume loss

421 in slate belts. Sorby (1856) initially suggested that a 50% volume reduction could occur in slates, but

422 settled on ~11% (1908). Wright and Platt (1982) suggested a volume loss of 50% in the Martinsburg

423 Shale of West Virginia. Similar volume reductions were suggested in the Taconic Slate Belt (Goldstein

424 et al., 1995, 1998). Onasch (1994) suggested a range of volume loss of 14-35% in deformed quartz

425 arenites. Similarly, Markley and Wojtal (1996) suggested 10-15% volume loss in an Appalachian mixed

426 siliciclastic sequence. Mosher (1987) analysed the variation in sizes of cobbles in the Purgatory

427 Conglomerate, Rhode Island, and suggested that there could be a volume loss of 23-55% of the original

428 cobble volumes in the areas of most intense deformation.

429 Despite these reports of significant volume reduction, these large volumes are rarely confirmed by

430 geochemical analyses (Wintsch et al., 1991; Erslev and Ward, 1994; Tan et al., 1995). Similarly, Ramsay

431 and Wood (1973) considered that a 10-20% volume reduction could occur based on density

432 differences between lithified mudstones and slates, and argued that greater volume losses were likely

433 to only occur in the deformation of incompletely consolidated sediments. As discussed earlier

434 shortening values of this magnitude have been identified by in a range of settings (e.g., Cooper et al.,

435 1983; Butler and Paton, 2010; Lathrop & Burberry, 2017).

436 While volume change has been mathematically incorporated into strain analysis (Gratier, 1983;

437 Onasch and Davis, 1988; Baird and Hudleston, 2007), most rocks lack the necessary strain markers for

438 this type of analysis. Some success has been made using isocon diagrams (Grant, 1986), but these are

439   typically restricted to discrete shear zones (Srivastava et al., 1995; Bhattacharyya and Hudleston,

440   2001; Baird and Hudleston, 2007). Other successes in identifying volume loss has come from gravity

441   driven fold and thrust belts, where the amount of extension high on the slope can be compared to the

442   amount of compression towards the toe of the slope (Butler and Paton, 2010).

443   **Conclusions**

444   Determining finite strain has seen significant developments since the seminal contribution of John

445   Ramsay. Through advances in imaging and software, it is easier than ever before to collect large data

446   sets and apply multiple strain analysis techniques rapidly, and there are a number of methods which

447   can incorporate statistical handling of the results. Strain analysis is regularly incorporated into

448   structural studies employing anisotropy of magnetic susceptibility, electron backscatter diffraction, x-

449   ray tomography, microstructural analysis etc., which have not only led to advances in our knowedge

450   of rock deformation processes, but also regional scale understanding. It should be obvious that

451   detailed strain analysis studies are required to understand the spatial variations of strain in deformed

452   terranes, but also the significance of those variations.

453   Of the many advances outlined here, most of them have been driven by developments in computing,

454   automation and statistical methods, whilst the basis for these strain analysis techniques have by in

455   large remained the same, which is a testament to the initial contribution of Ramsay. We anticipate

456   that the next significant advances in this field will again be largely technologically driven. In particular,

457   3D imaging of strain markers and 3D strain analysis should become more widespread, and perhaps

458   developed into 4D. Although, there have been advances in applying micro-tomography to geological

459   materials, these techniques are yet to be applied to strain analysis. There is also scope for advances

460   to be made in the extraction of high quality data from images with minimum human intervention e.g.,

461   grain boundary identification, and machine learning techniques could be applied to this. The natural

462   optical heterogeneity of geological materials, even in single mineral phases such as quartz due to

463   impurities, inclusions and microstructural features, will always makes the automation of grain

464   identification challenging. Increasingly the use of non-destructive chemical mapping techniques, for

465   example using electron microscope energy-dispersive X-Ray spectroscopy (QEMSCAN) or Raman

466   spectroscopy, produces outputs that allow the user to filter this heterogeneity thereby making the

467   process of grain boundary identification more manageable. This, coupled with new machine learning

468   techniques, will likely develop into a fully automated process for data acquisition, with strain analysis

469   studies becoming fully automated and significantly more efficient.

470   Regardless of any future developments, it should be clear that the strain analysis techniques of

471   Ramsay and their modernised equivalents should have a place in every structural geologist's toolbox.

472 **Acknowledgements**

477 **References**

478 Adam, J., Klinkmuiller, M., Schreurs, G., Wienke, B. 2013. Quantitative 3D strain analysis in analogue

479 experiments simulating tectonic deformation: Integration of X-ray computed tomography and digital

480 volume correlation techniques. Journal of Structural Geology, 55, 127-149.

481 Ailleres, L., Champenois, M., Macaudiere, J., Bertrand, J.., 1995. Use of image analysis in the

482 measurement of finite strain by the normalized Fry method: geological implications for the 'Zone

483 Houillere' (Brianconnais zone, French Alps). Mineralogical Magazine 59, 179–187

484 Asmussen, P., Conrad, O., Günther, A., Kirsch, M. and Riller, U., 2015. Semi-automatic segmentation

485 of petrographic thin section images using a "seeded-region growing algorithm" with an application to

486 characterize weathered subarkose sandstone. Computers & Geosciences, 83, pp.89-99.

487 Baird, G.B. and Hudleston, P.J., 2007. Modeling the influence of tectonic extrusion and volume loss on

488 the geometry, displacement, vorticity, and strain compatibility of ductile shear zones. Journal of

489 Structural Geology, 29(10), pp.1665-1678.

490 Barraud, J., 2006. The use of watershed segmentation and GIS software for textural analysis of thin

491 sections. Journal of Volcanology and Geothermal Research, 154(1-2), pp.17-33.

492 Bhattacharyya, P. and Hudleston, P., 2001. Strain in ductile shear zones in the Caledonides of northern

493 Sweden: a three-dimensional puzzle. Journal of Structural Geology, 23(10), pp.1549-1565.

494   Borradaile, G.J., 1976. A strain study of a granite–granite gneiss transition and accompanying

495   schistosity formation in the Betic orogenic zone, SE. Spain. Journal of the Geological Society, 132(4),

496   pp.417-428.

497   Borradaile, G., 1987. Anisotropy of magnetic susceptibility: rock composition versus strain.

498   Tectonophysics, 138(2-4), pp.327-329.

499   Borradaile, G.J. and Henry, B., 1997. Tectonic applications of magnetic susceptibility and its anisotropy.

500   Earth-Science Reviews, 42(1-2), pp.49-93.

501   Borradaile, G.J. and Jackson, M., 2004. Anisotropy of magnetic susceptibility (AMS): magnetic

502   petrofabrics of deformed rocks. Geological Society, London, Special Publications, 238(1), pp.299-360.

503   Boulter, C.A., 1976. Sedimentary fabrics and their relation to strain-analysis methods. Geology, 4(3),

504   pp.141-146.

505   Brandon, M.T., 1995. Analysis of geologic strain data in strain-magnitude space. Journal of Structural

506   Geology, 17(10), pp.1375-1385.

507   Breddin, H., 1954. Die tektonische Deformation der Fossilien im Rheinischen Schiefergebirge.

508   Zeitschrift der Deutschen Geologischen Gesellschaft, pp.227-305.

509   Breddin, H., 1957. Tektonische Fossil-und Gesteinsdeformation im Gebiet von St. Goarshausen

510   (Rheinisches Schiefergebirge): Decheniana, 110, pp.289-350.

511   Burberry, C.M., 2015. Spatial and temporal variation in penetrative strain during compression: Insights

512   from analog models. Lithosphere, 7(6), pp.611-624.

513   Burmeister, K.C., Harrison, M.J., Marshak, S., Ferré, E.C., Bannister, R.A. and Kodama, K.P., 2009.

514   Comparison of Fry strain ellipse and AMS ellipsoid trends to tectonic fabric trends in very low-strain

515   sandstone of the Appalachian fold–thrust belt. Journal of Structural Geology, 31(9), pp.1028-1038.

516 Butler, R.W.H. and Paton, D.A., 2010. Evaluating lateral compaction in deepwater fold and thrust belts:

517 How much are we missing from "nature's sandbox". GSA Today, 20(3), pp.4-10.

518 Cooper, M.A., Garton, M.R. and Hossack, J.R., 1983. The origin of the Basse Normandie duplex,

519 Boulonnais, France. Journal of Structural Geology, 5(2), pp.139-152.

520 Cloos, E., 1947. Oölite deformation in the South Mountain fold, Maryland. Geol. Soc. Am. Bull. 58,

521 843–918.

522 Choudhury, K.R., Meere, P.A. and Mulchrone, K.F., 2006. Automated grain boundary detection by

523 CASRG. Journal of Structural Geology, 28(3), pp.363-375.

524 Crespi, J.M., 1986. Some guidelines for the practical application of Fry's method of strain analysis.

525 Journal of Structural Geology, 8(7), pp.799-808.

526 Czeck, D.M., Fissler, D.A., Horsman, E. and Tikoff, B., 2009. Strain analysis and rheology contrasts in

527 polymictic conglomerates: an example from the Seine metaconglomerates, Superior Province,

528 Canada. Journal of Structural Geology, 31(11), pp.1365-1376.

529 De Paor, D.G., 1980. Some limitations of the Rf/ϕ technique of strain analysis. Tectonophysics, 64(1-

530 2), pp.T29-T31.

531 De Paor, D.G., 1988. Rf/øf strain analysis using an orientation net. Journal of Structural Geology, 10(4),

532 pp.323-333.

533 De Paor, D.G., 1990. Determination of the strain ellipsoid from sectional data. Journal of Structural

534 Geology, 12(1), pp.131-137.

535 DeSitter, L., 1964. Structural Geology. Mc Graw-Hill.

536 DeVasto, Michael A., Dyanna M. Czeck, and Prajukti Bhattacharyya. "Using image analysis and ArcGIS®

537 to improve automatic grain boundary detection and quantify geological images." Computers &

538 geosciences 49 (2012): 38-45.

539   Dunne, W.M., Onasch, C.M. and Williams, R.T., 1990. The problem of strain-marker centers and the

540   Fry method. Journal of Structural Geology, 12(7), pp.933-938.

541   Dunnet, D., 1969. A technique of finite strain analysis using elliptical particles. Tectonophysics 7, 117–

542   136.

543   Dunnet, D., Siddans, A., 1971. Non-random sedimentary fabrics and their modification by strain.

544   Tectonophysics 12, 307–325.

545   Elliott, D., 1970. Determination of finite strain and initial shape from deformed elliptical objects.

546   Geological Society of America Bulletin 81, 2221–2236.

547   Erslev, E., 1988. Normalized center-to-center strain analysis of packed aggregates. Journal of

548   Structural Geology 10, 201–209.

549   Erslev, E., Ge, H., 1990. Least-squares center-to-center and mean object ellipse fabric analysis. Journal

550   of Structural Geology 12, 1047–1059.

551   Erslev, E. A., & Ward, D. J. (1994). Non-volatile element and volume flux in coalesced slaty cleavage.

552   Journal of Structural Geology, 16(4), 531-553.

553   Flinn, D., 1956. On the deformation of the Funzie conglomerate, Fetlar, Shetland. J. Geol. 480–505.

554   Flinn, D., 1962a. On folding during three-dimensional progressive deformation. Q. J. Geol. Soc. 118.

555   Flinn, D., 1965. On the Symmetry Principle and the Deformation Ellipsoid. Geol. Mag. 102, 36–45.

556   Fossen, H., Tikoff, B. 1993. The deformation matrix for simultaneous simple shearing, pure shearing

557   and volume change, and its applications to transpression-transtension tectonics. Journal of Structural

558   Geology, 15, 413-422.

559   Freeman, B., 1987. The behaviour of deformable ellipsoidal particles in three-dimensional slow flows:

560   implications for geological strain analysis. Tectonophysics, 132(4), pp.297-309.

561   Freeman, B. and Lisle, R.J., 1987. The relationship between tectonic strain and the three-dimensional

562   shape fabrics of pebbles in deformed conglomerates. Journal of the Geological Society, 144(4), pp.635-

563   639.

564   Fry, N., 1979. Random point distributions and strain measurement in rocks. Tectonophysics 60, 89–

565   105.

566   Gay, N.C. 1968a Pure shear and simple shear deformation of inhomogenous viscous fluids. 1. Theory.

567   Tectonophysics 5, p 211-234.

568   Gay, N.C. 1968b Pure shear and simple shear deformation of inhomogenous viscous fluids. 2. The

569   determination of total finite strain in a rock from objects such as deformed pebbles. Tectonophysics

570   5, p 295-302.

571   Gay, N. C. 1969 The analysis of strain in the Barberton Mountain Land, Eastern Transvaal, using

572   deformed pebbles. Journal of Geology 77, p 377-396.

573   Gendzwill, D.J. and Stauffer, M.R., 1981. Analysis of triaxial ellipsoids: Their shapes, plane sections,

574   and plane projections. Journal of the International Association for Mathematical Geology, 13(2),

575   pp.135-152.

576   Goldstein, A., Pickens, J., Klepeis, K. and Linn, F., 1995. Finite strain heterogeneity and volume loss in

577   slates of the Taconic Allochthon, Vermont, USA. Journal of Structural Geology, 17(9), pp.1207-1216.

578   Goldstein, A., Knight, J. and Kimball, K., 1998. Deformed graptolites, finite strain and volume loss

579   during cleavage formation in rocks of the taconic slate belt, New York and Vermont, USA. Journal of

580   structural geology, 20(12), pp.1769-1782.

581   Goodchild, J.S. and Fueten, F., 1998. Edge detection in petrographic images using the rotating polarizer

582   stage. Computers & Geosciences, 24(8), pp.745-751.

583   Gorsevski, P.V., Onasch, C.M., Farver, J.R. and Ye, X., 2012. Detecting grain boundaries in deformed

584   rocks using a cellular automata approach. Computers & Geosciences, 42, pp.136-142.

585   Grant, J.A., 1986. The isocon diagram; a simple solution to Gresens' equation for metasomatic

586   alteration. Economic geology, 81(8), pp.1976-1982.

587   Gratier, J.P., 1983. Estimation of volume changes by comparative chemical analyses in

588   heterogeneously deformed rocks (folds with mass transfer). In Strain Patterns in Rocks (pp. 329-339).

589   Hanna, S., Fry, N., 1979. A comparison of methods of strain determination in rocks from southwest

590   Dyfed (Pembrokeshire) and adjacent areas. Journal of Structural Geology 1, 155–162.

591   Haughton, S., 1856. LII. On slaty cleavage, and the distortion of fossils. London, Edinburgh, Dublin

592   Philos. Mag. J. Sci. 12, 409–421.

593   Heilbronner, R., 2000. Automatic grain boundary detection and grain size analysis using polarization

594   micrographs or orientation images. Journal of Structural Geology 22, 969–981.

595   Heilbronner, R. and Barrett, S., 2013. Image analysis in earth sciences: microstructures and textures

596   of earth materials (Vol. 129). Springer Science & Business Media.

597   Hobbs, B.E. and Talbot, J.L., 1966. The analysis of strain in deformed rocks. The Journal of Geology,

598   74(4), pp.500-513.

599   Hobbs, B.E., Means, W.D. and Williams, P.F., 1976. An outline of structural geology. Wiley.

600   Holst, T.B., 1982. The role of initial fabric on strain determination from deformed ellipsoidal objects.

601   Tectonophysics, 82(3-4), pp.329

602   Hossack, J.R., 1968. Pebble deformation and thrusting in the Bygdin area (southern Norway).

603   Tectonophysics, 5(4), pp.315-339.-350.

604   Hsu, T.C., 1966. The characteristics of coaxial and non-coaxial strain paths. Journal of Strain Analysis,

605   1(3), pp.216-222.

606   Jungmann, M., Pape, H., Wißkirchen, P., Clauser, C. and Berlage, T., 2014. Segmentation of thin section

607   images for grain size analysis using region competition and edge-weighted region merging. Computers

608   & Geosciences, 72, pp.33-48.

609   Koyi, H.A., Sans, M., Teixell, A., Cotton, J. and Zeyen, H., 2004. The significance of penetrative strain in

610   the restoration of shortened layers—Insights from sand models and the Spanish Pyrenees. In K. R.

611   McClay, ed., Thrust tectonics and hydrocarbon systems: AAPG Memoir 82, p. 1–16.

612   Kumar, R., Srivastava, D.C. and Ojha, A.K., 2014. A comparison of the methods for objective strain

613   estimation from the Fry plots. Journal of Structural Geology, 63, pp.76-90.

614   Lathrop, B.A. and Burberry, C.M., 2017. Accommodation of penetrative strain during deformation

615   above a ductile décollement. Lithosphere, 9(1), pp.46-57.

616   Launeau, P., Bouchez, J.L. and Benn, K., 1990. Shape preferred orientation of object populations:

617   automatic analysis of digitized images. Tectonophysics, 180(2-4), pp.201-211.

618   Launeau, P.A., and Robin, P.Y., 1996. Fabric analysis using the intercept method. Tectonophysics,

619   267(1-4), pp.91-119.

620   Launeau, P. and Robin, P.Y.F., 2005. Determination of fabric and strain ellipsoids from measured

621   sectional ellipses—Implementation and applications. Journal of Structural Geology, 27(12), pp.2223-

622   2233.

623   Launeau, P., Archanjo, C.J., Picard, D., Arbaret, L. and Robin, P.Y., 2010. Two-and three-dimensional

624   shape fabric analysis by the intercept method in grey levels. Tectonophysics, 492(1-4), pp.230-239.

625   Law, R.D., 1986. Relationships between strain and quartz crystallographic fabrics in the Roche Maurice

626   quartzites of Plougastel, western Brittany. Journal of Structural Geology, 8(5), pp.493-515.

627   Leeder, M.R., 1982. Sedimentology: process and product. Springer.

628   Li, Y., Onasch, C.M. and Guo, Y., 2008. GIS-based detection of grain boundaries. Journal of Structural

629   Geology, 30(4), pp.431-443.

630   Lisle, R., 1977a. Estimation of the tectonic strain ratio from the mean shape of deformed elliptical

631   objects. Geologie en Mijnbouw 56, 140–144.

632   Lisle, R., 1977b. Clastic grain shape and orientation in relation to cleavage from the Aberystwyth Grits,

633   Wales. Tectonophysics 39, 381–395.

634   Lisle, R.J., Rondeel, H.E., Doorn, D., Brugge, J. and Van de Gaag, P., 1983. Estimation of viscosity

635   contrast and finite strain from deformed elliptical inclusions. Journal of Structural Geology, 5(6),

636   pp.603-609.

637   Lisle, R., 1985. Geological Strain Analysis: A Manual for the Rf/φ Method. Pergamon Press.

638   Lisle, R.J., 1985b. The effect of composition and strain on quartz-fabric intensity in pebbles from a

639   deformed conglomerate. Geologische Rundschau, 74(3), pp.657-663.

640   Lisle,R., 1994. Palaeostrain Analysis. In P.L. Hancock (Ed.), Continental Deformation, Pergamon Press,

641   pp. 28-42.

642   Lisle, R.J., 2010. Strain analysis from point fabric patterns: An objective variant of the Fry method.

643   Journal of Structural Geology, 32(7), pp.975-981.

644   Louis, L., Wong, T., Buad, P. Tembe, S. 2006. Imaging strain localization by X-ray computed

645   tomography: discrete compaction bands in Diemelstadt sandstone. Journal of Structural Geology, 28,

646   762-775.

647   Maffione, M. and Morris, A., 2017. The onset of fabric development in deep marine sediments. Earth

648   and Planetary Science Letters, 474, pp.32-39.

649 Mandal, N., Samanta, S.K., Bhattacharyya, G. and Chakraborty, C., 2003. Deformation of ductile

650 inclusions in a multiple inclusion system in pure shear. Journal of Structural Geology, 25(9), pp.1359-

651 1370.

652 Marjoribanks, R.W., 1976. The relation between microfabric and strain in a progressively deformed

653 quartzite sequence from central Australia. Tectonophysics, 32(3-4), pp.269-293.

654 Markley, M. and Wojtal, S., 1996. Mesoscopic structure, strain, and volume loss in folded cover strata,

655 Valley and Ridge Province, Maryland. American Journal of Science, 296(1), pp.23-57.

656 Masuda, T., Koike, T., Yuko, T. and Morikawa, T., 1991. Discontinuous grain growth of quartz in

657 metacherts: the influence of mica on a microstructural transition. Journal of Metamorphic Geology,

658 9(4), pp.389-402.

659 Matthews, P.E., Bond, R.A.B. and Van Den Berg, J.J., 1974. An algebraic method of strain analysis using

660 elliptical markers. Tectonophysics, 24(1-2), pp.31-67.

661 McCarthy, D.J., Meere, P.A. and Petronis, M.S., 2015. A comparison of the effectiveness of clast based

662 finite strain analysis techniques to AMS in sandstones from the Sevier Thrust Belt, Wyoming.

663 Tectonophysics, 639, pp.68-81.

664 McNaught, M, 1994. Modifying the normalized Fry method for aggregates of non-elliptical grains.

665 Journal of Structural Geology, 16(4), pp.493-503.

666 Means, W.D., Hobbs, B.E., Lister, G.S., Williams, P.F. 1980. Vorticity and non-coxiality in progressive

667 deformation. Journal of Structural Geology, 2, 371-378.

668 Meere, P.A., Mulchrone, K.F., Sears, J.W. and Bradway, M.D., 2008. The effect of non-passive clast

669 behaviour in the estimation of finite strain in sedimentary rocks. Journal of Structural Geology, 30(10),

670 pp.1264-1271.

671   Meere, P.A., Mulchrone, K.F., McCarthy, D.J., Timmerman, M.J. and Dewey, J.F., 2016. Prelithification

672   and synlithification tectonic foliation development in a clastic sedimentary sequence. Geology, 44(4),

673   pp.291-294.

674   Miller, D.M. and Christie, J.M., 1981. Comparison of quartz microfabric with strain in recrystallized

675   quartzite. Journal of Structural Geology, 3(2), pp.129-141.

676   Milton, N.J., 1980. Determination of the strain ellipsoid from measurements on any three sections.

677   Tectonophysics, 64(1-2), pp.T19-T27.

678   Mingireanov Filho, I., Spina, T.V., Falcão, A.X. and Vidal, A.C., 2013. Segmentation of sandstone thin

679   section images with separation of touching grains using optimum path forest operators. Computers &

680   Geosciences, 57, pp.146-157.

681   Mitra, G., 1994. Strain variation in thrust sheets across the Sevier fold-and-thrust belt (Idaho-Utah-

682   Wyoming): Implications for section restoration and wedge taper evolution. Journal of Structural

683   Geology, 16(4), pp.585-602.

684   Mookerjee, M., Nickleach, S., 2011. Three-dimensional strain analysis using Mathematica. J. Struct.

685   Geol. 33, 1467–1476.

686   Mookerjee, M. and Peek, S., 2014. Evaluating the effectiveness of Flinn's k-value versus Lode's ratio.

687   Journal of Structural Geology, 68, pp.33-43.

688   Mosher, S., 1987. Pressure-solution deformation of the Purgatory Conglomerate, Rhode Island (USA):

689   quantification of volume change, real strains and sedimentary shape factor. Journal of structural

690   geology, 9(2), pp.221-232.

691   Mukul, M., 1998. A spatial statistics approach to the quantification of finite strain variation in

692   penetratively deformed thrust sheets: an example from the Sheeprock Thrust Sheet, Sevier. Journal

693   of Structural Geology20, 371–384.

694   Mulchrone, K.F. and Meere, P.A., 2001. A Windows program for the analysis of tectonic strain using

695   deformed elliptical markers. Computers & geosciences, 27(10), pp.1251-1255.

696   Mulchrone, K.F., 2003. Application of Delaunay triangulation to the nearest neighbour method of

697   strain analysis. Journal of Structural Geology, 25(5), pp.689-702.

698   Mulchrone, K.F., O'Sullivan, F. and Meere, P.A., 2003. Finite strain estimation using the mean radial

699   length of elliptical objects with bootstrap confidence intervals. Journal of Structural Geology, 25(4),

700   pp.529-539.

701   Mulchrone, K.F., Meere, P.A. and Choudhury, K.R., 2005. SAPE: a program for semi-automatic

702   parameter extraction for strain analysis. Journal of structural geology, 27(11), pp.2084-2098.

703   Mulchrone, K.F. and Walsh, K., 2006. The motion of a non-rigid ellipse in a general 2D deformation.

704   Journal of Structural Geology, 28(3), pp.392-407.

705   Mulchrone, K.F., 2013. Fitting the void: Data boundaries, point distributions and strain analysis.

706   Journal of Structural Geology, 46, pp.22-33.

707   Mulchrone, K.F., McCarthy, D.J. and Meere, P.A., 2013. Mathematica code for image analysis, semi-

708   automatic parameter extraction and strain analysis. Computers & Geosciences, 61, pp.64-70.

709   Nádai, A., 1950. Theory of flow and fracture of solids, v. 2.

710   Oertel, G., 1978. Strain determination from the measurement of pebble shapes. Tectonophysics,

711   50(1), pp.T1-T7.

712   Onasch, C.M., 1986. Ability of the Fry method to characterize pressure-solution deformation.

713   Tectonophysics, 122(1-2), pp.187-193.

714   Onasch, C.M., 1994. Assessing brittle volume-gain and pressure solution volume-loss processes in

715   quartz arenite. Journal of Structural Geology, 16(4), pp.519-530.

716   Onasch, C.M. and Davis, T.L., 1988. Strain determination using cathodoluminescence of calcite

717   overgrowths. Journal of structural geology, 10(3), pp.301-303.

718   Owens, W.H., 1984. The calculation of a best-fit ellipsoid from elliptical sections on arbitrarily

719   orientated planes. J. Struct. Geol. 6, 571–578.

720   Panozzo, R., 1984. Two-dimensional strain from the orientation of lines in a plane. Journal of Structural

721   Geology 6, 215–221.

722   Panozzo, R., 1987. Two-dimensional strain determination by the inverse SURFOR wheel. Journal of

723   Structural Geology, 9(1), pp.115-119.

724   Park, R.G., 1997. Foundation of structural geology. Routledge.

725   Passchier, C.W. and Trouw, R.A., 2005. Microtectonics (Vol. 1). Springer Science & Business Media.

726   Paterson, S., Yu, H., 1994. Primary fabric ellipsoids in sandstones: implications for depositional

727   processes and strain analysis. J. Struct. Geol. 16, 505–517.

728   Peach, C., and Lisle, R., 1979. A Fortran IV program for the analysis of tectonic strain using deformed

729   elliptical markers. Computers & Geosciences 5, 325–334.

730   Perring, C.S., Barnes, S.J., Verrall, M. and Hill, R.E.T., 2004. Using automated digital image analysis to

731   provide quantitative petrographic data on olivine–phyric basalts. Computers & Geosciences, 30(2),

732   pp.183-195.

733   Phillips, J., 1843. On certain movements in the parts of stratified rocks. Adv. Sci, pp.60-61.

734   Prior, D.J., Mariani, E. and Wheeler, J., 2009. EBSD in the earth sciences: applications, common

735   practice, and challenges. In Electron backscatter diffraction in materials science (pp. 345-360).

736   Springer, Boston, MA.

737   Protzman, G.M. and Mitra, G., 1990. Strain fabric associated with the Meade thrust sheet: implications

738   for cross-section balancing. Journal of Structural Geology, 12(4), pp.403-417.

739   Ramsay, J.G., 1967. Folding and fracturing of rocks. New York, MacGraw-Hill, 568p

740   Ramsay, J.G. and Wood, D.S., 1973. The geometric effects of volume change during deformation

741   processes. Tectonophysics, 16(3-4), pp.263-277.

742   Ramsay, J.G., and Huber, M., 1983. The techniques of modern structural geology. Strain Analysis,

743   London: Academic Press.

744   Reddy, B.S.R. and Srivastava, D.C., 2012. Rapid extraction of central vacancy by image-analysis of Fry

745   plots. Journal of Structural Geology, 40, pp.44-53.

746   Robin, P., 1977. Determination of geologic strain using randomly oriented strain markers of any shape.

747   Tectonophysics 42, T7–T16.

748   Robin, P.-Y.F., 2002. Determination of fabric and strain ellipsoids from measured sectional ellipses —

749   theory. J. Struct. Geol. 24, 531–544.

750   Robin P.F., Charles, C.R.J. 2015. Quantifying the three-dimensional shapes of spheroidal objects in

751   rocks imaged by tomography. Journal of Structural Geology, 77, 1-10.

752   Seymour, D.B. and Boulter, C.A., 1979. Tests of computerised strain analysis methods by the analysis

753   of simulated deformation of natural unstrained sedimentary fabrics. Tectonophysics, 58(3-4), pp.221-

754   235.

755   Shan, Y., 2008. An analytical approach for determining strain ellipsoids from measurements on planar

756   surfaces. Journal of Structural Geology, 30(4), pp.539-546

757   Shan, Y. and Xiao, W., 2011. A statistical examination of the Fry method of strain analysis. Journal of

758   Structural Geology, 33(5), pp.1000-1009.

759   Shao, J. and Wang, C., 1984. Determination of strain ellipsoid according to two-dimensional data on

760   three or more intersection planes. Journal of the International Association for Mathematical Geology,

761   16(8), pp.823-833.

762   Sharpe, D., 1847. On slaty cleavage. Q. J. Geol. Soc. 3, 74–105.

763   Shimamoto, T., Ikeda, Y., 1976. A simple algebraic method for strain estimation from deformed
764   ellipsoidal objects. 1. Basic theory. Tectonophysics 36, 315–337.

765   Siddans, A.W.B., 1980. Analysis of three-dimensional, homogeneous, finite strain using ellipsoidal
766   objects. Tectonophysics, 64(1-2), pp.1-16.

767   Soares, A. and Dias, R., 2015. Fry and Rf/φ strain methods constraints and fold transection
768   mechanisms in the NW Iberian Variscides. Journal of Structural Geology, 79, pp.19-30.

769   Sorby, H., 1849. On the origin of slaty cleavage. Proc. Geol. Polytech. Soc. West Rid. Yorksh. 3, 300–
770   312.

771   Sorby, H., 1856. XVIII. On the theory of the origin of slaty cleavage. London, Edinburgh, Dublin Philos.
772   Mag. J. Sci. 12, 127–129.

773   Sorby, H.C., 1908. On the application of quantitative methods to the study of the structure and history
774   of rocks. Quarterly Journal of the Geological Society, 64(1-4), pp.171-233.

775   Srivastava, H.B., Hudleston, P. and Earley III, D., 1995. Strain and possible volume loss in a high-grade
776   ductile shear zone. Journal of Structural Geology, 17(9), pp.1217-1231.

777   Tan, B.K., Gray, D.R. and Stewart, I., 1995. Volume change accompanying cleavage development in
778   graptolitic shales from Gisborne, Victoria, Australia. Journal of Structural Geology, 17(10), pp.1387-
779   1394.

780   Tarquini, S. and Favalli, M., 2010. A microscopic information system (MIS) for petrographic analysis.
781   Computers & Geosciences, 36(5), pp.665-674.

782   Tikoff, B, Fossen, H. 1993. Simultaneous pure and simple shear: the unifying deformation matrix.
783   Tectonophysics, 217, 267-283.

784   Tikoff, B, Fossen, H. 1995. The limitations of three dimensional kinematic vorticity analysis. Journal of

785   Structural Geology, 17, 1771-1784.

786   Tikoff, B, Fossen, H. 1999. Three dimensional reference deformations and strain facies. Journal of

787   Structural Geology, 21, 1497-1512.Todd, S.P., 2000, Taking the roof off a suture zone: basin setting

788   and provenance of conglomerates in the ORSDingle Basin of SW Ireland: Geological Society, London,

789   Special Publications, v. 180, no. 1, p. 185–222.

790   Treagus, S.H., 2002. Modelling the bulk viscosity of two-phase mixtures in terms of clast shape. Journal

791   of Structural Geology, 24(1), pp.57-76.

792   Treagus, S.H., and Treagus, J.E., 2002. Studies of strain and rheology of conglomerates. J. Struct. Geol.

793   24, 1541–1567.

794   Van den Berg, E.H., Meesters, A.G.C.A., Kenter, J.A.M. and Schlager, W., 2002. Automated separation

795   of touching grains in digital images of thin sections. Computers & Geosciences, 28(2), pp.179-190.

796   Vitale, S. and Mazzoli, S., 2005. Influence of object concentration on finite strain and effective viscosity

797   contrast: insights from naturally deformed packstones. Journal of Structural Geology, 27(12), pp.2135-

798   2149.

799   Vollmer, F. W., 2010. A comparison of ellipse-fitting techniques for two and three-dimensional strain

800   analysis, and their implementation in an integrated computer program designed for field-based

801   studies. Abstract T21B-2166, Fall Meeting, American Geophysical Union, San Francisco, California.

802   Vollmer, F. W., 2011. Best-fit strain from multiple angles of shear and implementation in a computer

803   program for geological strain analysis. Geological Society of America Abstracts with Programs, v. 43.

804   Vollmer, F. W., 2017. EllipseFit: Strain and Fabric Analysis Software User Manual Version 3.4.0

805   [computer software user manual]. Retrieved from http://www.frederickvollmer.com/ellipsefit/.

806   Waldron, J.W. and Wallace, K.D., 2007. Objective fitting of ellipses in the centre-to-centre (Fry)

807   method of strain analysis. Journal of Structural Geology, 29(9), pp.1430-1444.

808   Weil, A.B. and Yonkee, A., 2009. Anisotropy of magnetic susceptibility in weakly deformed red beds

809   from the Wyoming salient, Sevier thrust belt: Relations to layer-parallel shortening and orogenic

810   curvature. Lithosphere, 1(4), pp.235-256.

811   Wheeler, J., 1986. Strain analysis in rocks with pretectonic fabrics. Journal of structural geology, 8(8),

812   pp.887-896.

813   Wintsch, R.P., Kvale, C.M. and Kisch, H.J., 1991. Open-system, constant-volume development of slaty

814   cleavage, and strain-induced replacement reactions in the Martinsburg Formation, Lehigh Gap,

815   Pennsylvania. Geological Society of America Bulletin, 103(7), pp.916-927.

816   Woodward, N.B., Gray, D.R. and Spears, D.B., 1986. Including strain data in balanced cross-sections.

817   Journal of Structural Geology, 8(3-4), pp.313-324.

818   Wright, T.O. and Platt, L.B., 1982. Pressure dissolution and cleavage in the Martinsburg Shale.

819   American Journal of Science, 282(2), pp.122-135.

820   Yu, H., Zheng, Y., 1984. A statistical analysis applied to the R_f/φ method. Tectonophysics 110, 151–

821   155.

822   Zingg, T., 1935. Beitrag zur schotteranalyse (Doctoral dissertation, ETH Zurich).

823

824

Figure Captions

826 Fig. 1 Identifying strain in rocks. A. A highly idealised rock outcrop with three exposed mutually

827 perpendicular surfaces, with appropriate strain markers on each surface. The strain ellipsoid illustrates

828 the relationship between the tectonic stretching axes XYZ and sigma 1, 2 & 3. B. A real outcrop from

829 the Dingle Peninsula, which presents a more challenging problem for identifying and quantifying

830 strain.

831 Fig. 2 A. Measuring the long (M) and short (m) axes of elliptical strain markers. B. Plot of the long and

832 short axes from A. The slope of a best-fit line that passes through the points and the origin provides

833 an estimate of the strain ratio. C. Measuring chords along three defined directions for a population of

834 ellipses.

835 Fig. 3 Nearest-neighbour and or centre-to-centre methodology. A. Centre to centre techniques are

836 based on the assumption that the tie-lines between nearest neighbours have a uniformly random

837 distribution in the unstrained state. The lengths, d, and orientations, α, of tie lines joining object

838 centres are marked. The Polar plot of the unstrained state is illustrated below, showing d vs α.

839 Interestingly, this unstrained sample has a weak preferred distribution, in that the clasts are closer

840 together in the vertical direction than the horizontal direction. B. Initial strained state, the distances

841 between clasts become shorter in the tectonic shortening direction. The polar plot indicates higher

842 strain estimates. The apex of the curve shows the orientation of the longest direction and the nadir

843 shows the orientation of the shortest direction. C. The final strain state with pressure solution and a

844 higher strain estimate.

845 Fig. 4 The Rf/Ø method. A. After fitting ellipses to strain markers, the ratio of the long axis to short

846 axis is calculated and the orientation relative to a reference angle is recorded. B. These ratios are then

847 plotted against the orientation of the long axis. This limited data set suggests that preferred

848 orientation is between 45 degrees and 75 degrees. Clearly more data is required to more accurately
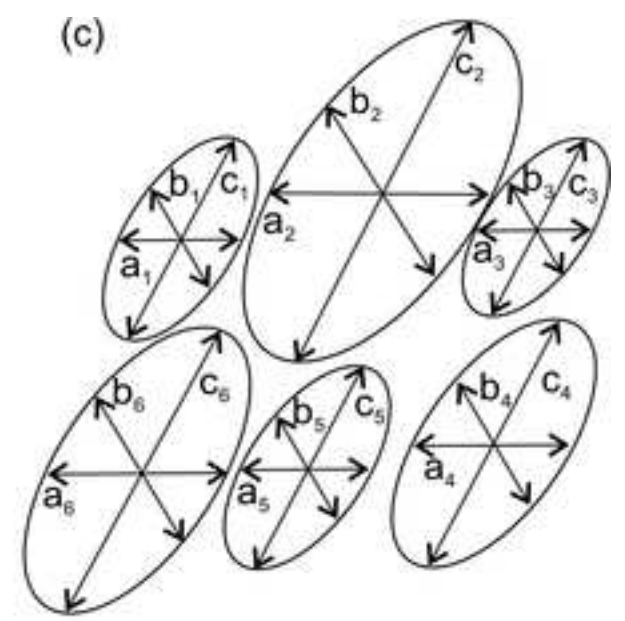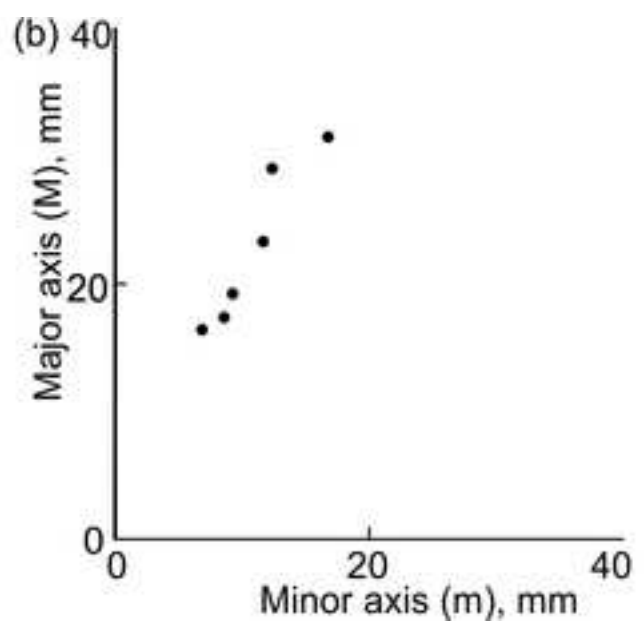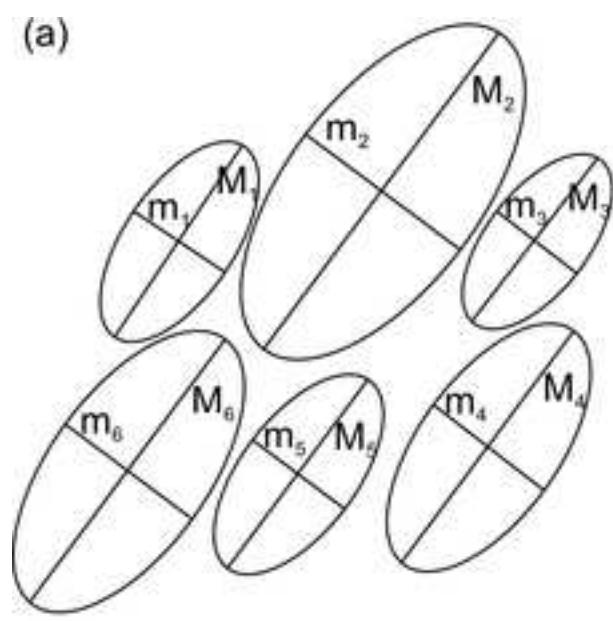
849 estimate strain.

850   Fig. 5. Flinn and Nadai-Hsu plots. A. Flinn plots represent all possible ellipsoid geometries in a 2D space.

851   The standard convention is to use a logarithmic plot, where the ratio of the maximum to intermediate

852   ellipsoid axes (Ln X/Y) is plotted as ordinate and the ratio of the minimum to intermediate axes (Ln

853   Y/Z) is plotted as abscissa. Prolate spheroids plot along the vertical axis and oblate spheroids plot along

854   the horizontal. As these ellipsoids become less spherical, they plot further away from the origin. B.

855   Nadai-Hsu plots show similar information to the Flinn Plots, but have an advantage that less deformed

856   ellipsoids plot closer together regardless of shape.

857   Fig. 6. Typical strain analysis methodology. A. Selection of a suitable oriented thin section. B. Fitting

858   ellipses to the clasts shown in A. C. Fitting the central void of the Fry Plot. D. The same data is

859   presented in a polar plot. E. Strain estimate from the DTNNM method represented by the black star.

860   The shaded ellipses represent the Bootstrapped confidence intervals. F. Strain estimate from the MRL

861   method represented by the black star. The shaded ellipses represent the Bootstrapped confidence

862   intervals. Note the underestimate compared to the DTNNM method.
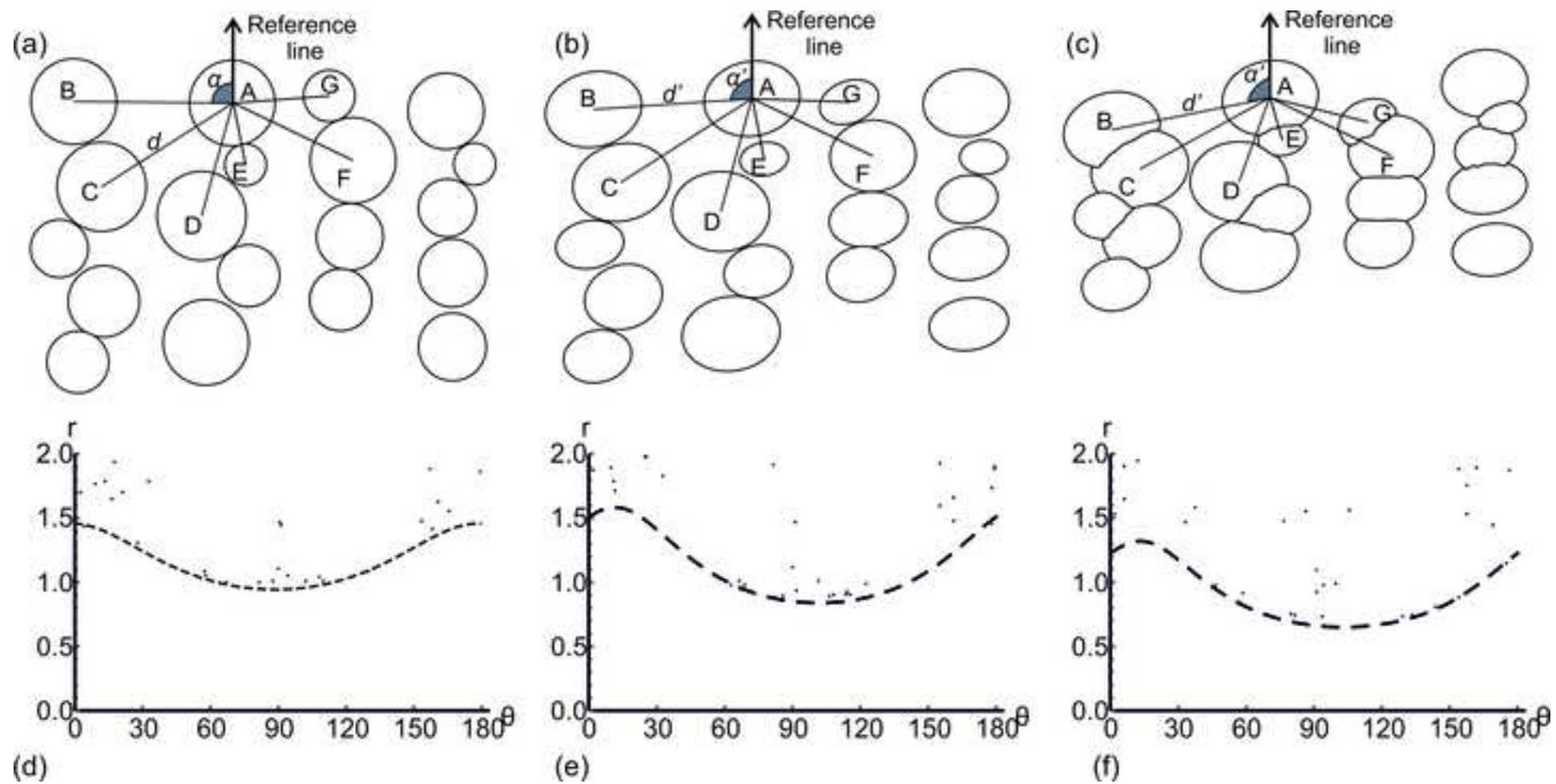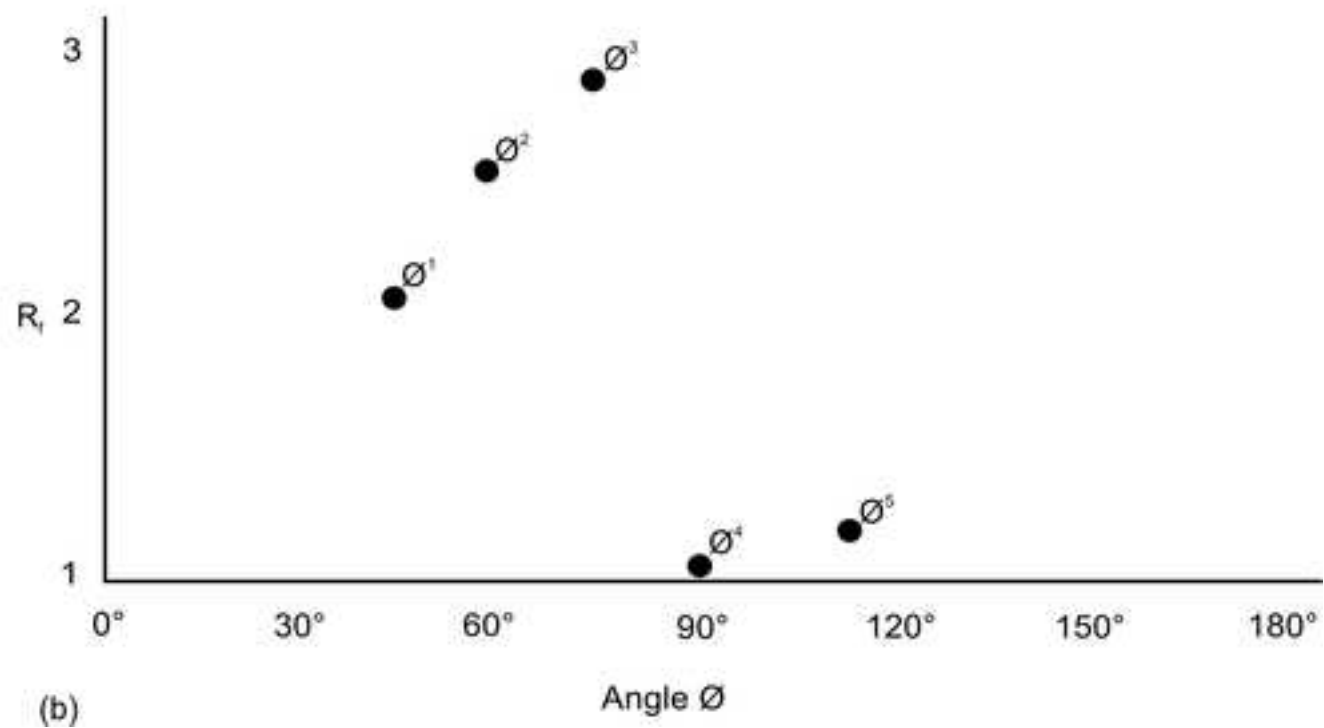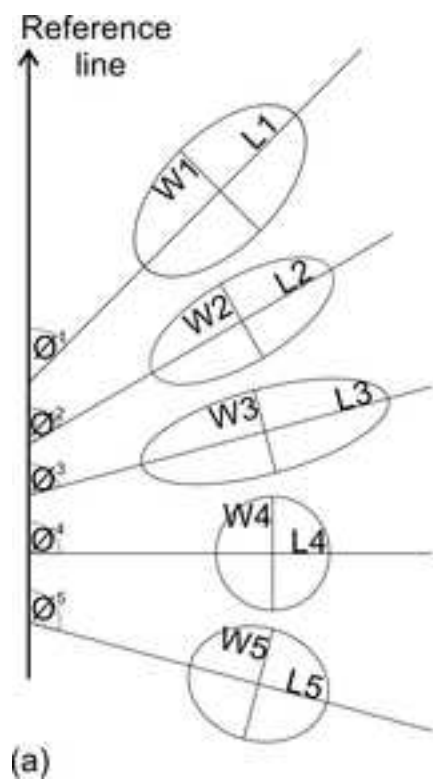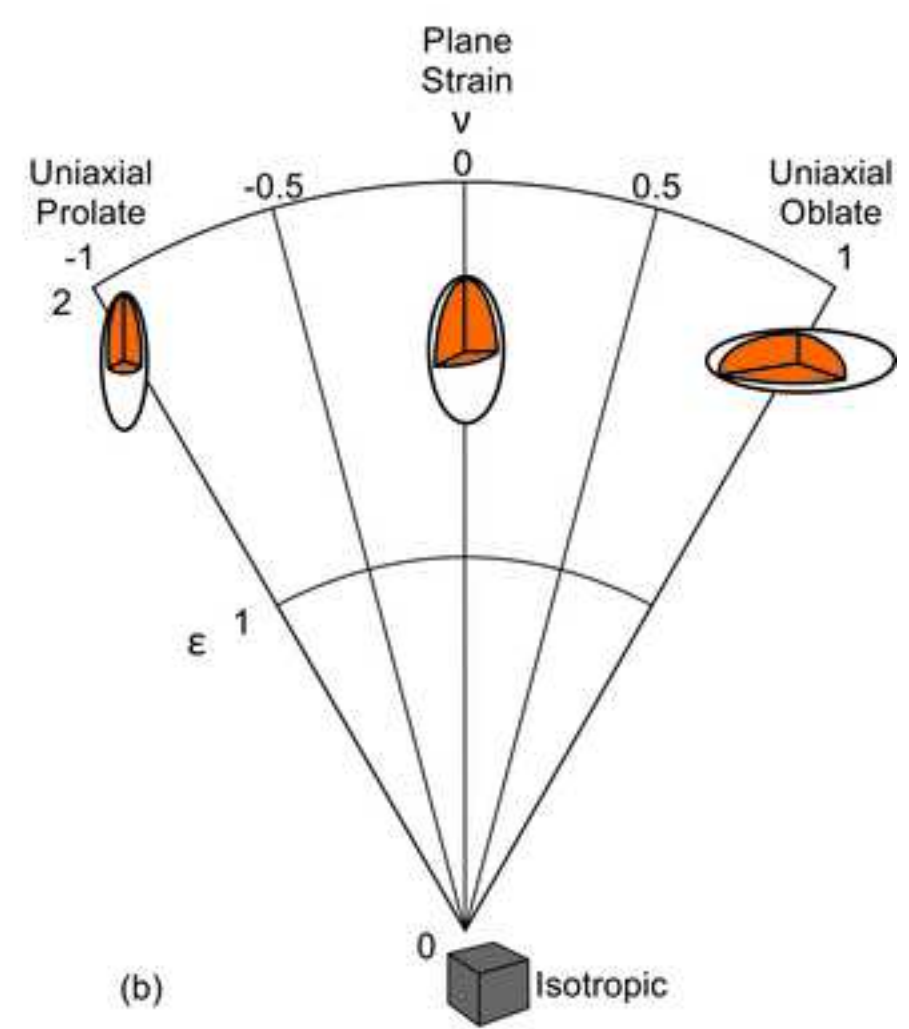
Figure

Figure

(a)

(b)

(c)

Figure

Figure

Reference line

W1 L1

W2 L2

W3 L3

W4 L4

W5 L5

$\emptyset^1$
$\emptyset^2$
$\emptyset^3$
$\emptyset^4$
$\emptyset^5$

(a)

3

R_f 2

1

0° 30° 60° 90° 120° 150° 180°

Angle $\emptyset$

$\emptyset^1$
$\emptyset^2$
$\emptyset^3$
$\emptyset^4$
$\emptyset^5$

(b)

Figure

(a)

(b)

(c)

(d)

(e)

(f)